Sensors and Actuators B 206 (2015) 56–64

Contents lists available at ScienceDirect

Sensors and Actuators B: Chemical

journal homepage: www.elsevier.com/locate/snb

Hybridization-induced suppression of coffee ring effect for nucleic acid detection

Yuanhang Li[a,1], Zichen Zhao[b,1], Miu Ling Lam[c,d], Wei Liu[b], Pak Piu Yeung[b], Ching-Chang Chieng[b], Ting-Hsuan Chen[b,c,d,*]

[a] Department of Electronic Engineering, City University of Hong Kong, Hong Kong Special Administrative Region
[b] Department of Mechanical and Biomedical Engineering, City University of Hong Kong, Hong Kong Special Administrative Region
[c] School of Creative Media, City University of Hong Kong, Hong Kong Special Administrative Region
[d] Centre for Robotics and Automation, City University of Hong Kong, Hong Kong Special Administrative Region

ARTICLE INFO

Article history:
Received 13 August 2014
Accepted 2 September 2014
Available online 16 September 2014

Keywords:
Coffee ring effect
Nucleic acid
Cheerios effect

ABSTRACT

We demonstrate a method for the detection of nucleic acid using hybridization-induced suppression of the coffee ring effect. When a sessile droplet is pinned on a solid surface, evaporation induces an outward capillary flow that moves suspended particles toward the periphery of the droplet and leaves a ring-shape structure. Compared with spherical particles that are carried to the contact line and form rings, non-spherical particles tend to adhere to each other at the air–water interface where they gain enhanced resistance to the capillary flow and suppress the coffee ring effect. Here, we used suspended microspheres surface-functionalized with single-strand oligonucleotide probes that were complementary to a target DNA. The present target DNA hybridized with the oligonucleotide probe and connected with multiple microspheres, leading to the generation of non-spherical particle agglomerates that resist the capillary flow and form a more uniform deposition of particles after evaporation. Video microscopy and numerical simulation showed that the suppression is because non-spherical particle agglomerates distorted the meniscus surrounding them and exerted a long-range capillary attraction that enhanced the fluidic resistance. Eventually, the microscale hybridization events were translated into the change of coffee ring patterns at macroscale. Using coffee rings as the readout, proof-of-principle studies showed effective sensitivity at low concentrations of 10–100 nM with a wide dynamic range from 10^{-5} M to 10^{-8} M, and high specificity that can distinguish the sequence with a single mismatched nucleotide. Owing to the simplicity of the operation and visual readout without the need of a special detector, our approach demonstrates immense potential for the inexpensive and convenient detection of nucleic acid in at resources-limited settings.

1. Introduction

The detection of nucleic acid is of great interest in broad applications such as diseases diagnostics [1–3], identification of pathogens [4–6], and monitoring environmental safety [7]. For example, seven signature mRNAs elevated in saliva were reported to be an effective biomarker for oral cancer [1]. When analyzing pathogenicity, chromosomal markers with species-specific sequences can be also used to differentiate pathogenic strains [4–6], which is important for food safety and homeland security when faced with bioterrorism threats. To date, the gold standard for detecting nucleic acid has been the polymerase chain reaction (PCR). However, PCR requires sophisticated sample preparation, expensive laboratory instrumentation, and fully trained operators, which are unavailable in many situations, such as local clinics or sites for collecting environmental samples. Accordingly, there is a strong demand for platforms that are simple, inexpensive, and user-friendly. Toward this end, miniaturized formats have been adopted in platforms such as microfluidic-based PCR [5,8], electrochemistry based microfluidic sensors [9,10], and colorimetric assays using nanoparticles [2,11–15] or quantum dots [4,16]. However, cumbersome components (pumps, valves, current meter, or power supplier) and complicated setups are unavoidable in most systems. Efforts are still needed to simplify the detection method further.

The coffee ring effect is a natural phenomenon frequently observed in daily life. When a sessile drop containing suspended substances is pinned on a solid surface, a ring-shaped structure

* Corresponding author. Tel.: +852 3442 4114; fax: +852 3442 0172.
E-mail address: thchen@cityu.edu.hk (T.-H. Chen).
[1] These authors contributed equally to this work.

http://dx.doi.org/10.1016/j.snb.2014.09.006
0925-4005/

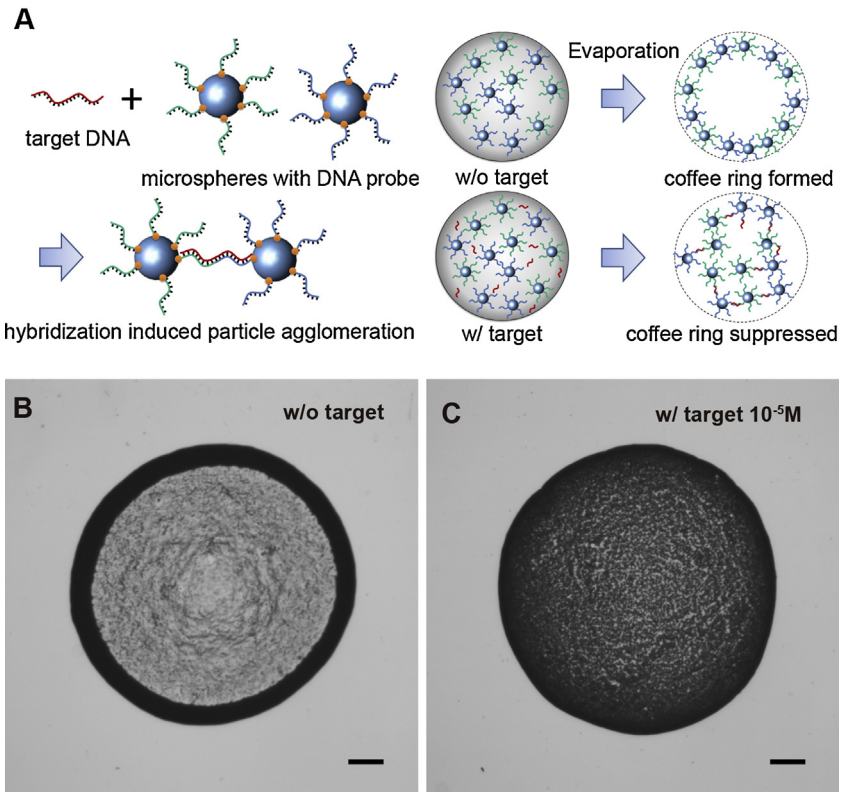

Fig. 1. Detection of target DNA using the coffee ring effect. (A) Schematics of the sensing mechanism. With microspheres functionalized with to $P1_{rpoB}$ (blue) or $P2_{rpoB}$ (green) that have a complementary sequence with the target DNA, rpoB (red), in juxtaposition, the target DNA rpoB can bridge two microspheres together (left). After evaporation, the droplet with no target DNA forms a perfect coffee ring at its edge, whereas the droplet with target DNA deposits the microspheres more uniformly (right). (B) Without target DNA, rpoB, the microspheres form a coffee ring. (C) When target DNA is present at a concentration of 10^{-5} M, the microspheres are uniformly deposited after evaporation. (For interpretation of the references to color in this figure legend, the reader is referred to the web version of this article.)

is formed after evaporation. The effect is driven by the maximum evaporative flux that occurs around the periphery of the sessile drop and the pinning effect that prevents receding of the contact line [17–19]. As a result, a radial, outward capillary flow is established to replenish the increased removal of solvent at the periphery. This phenomenon concentrates the suspended particles at the rim, eventually leaving a ring-shape structure after drying [17,18]. The coffee ring effect has gained increased attention due to its intriguing physics [17,18,20] and applications for paint manufacture, ink jet printing [21], and particle assembly [22]. In many cases, the coffee ring effect is undesired because it causes a non-uniform deposition of entities. Extensive attempts have been made to eliminate the coffee ring effect using the Marangoni effect [23], capillary repulsion [24], addition of surfactant [25], and control of the droplet size [20]. In contrast, earlier studies were also made to take advantage on the self-driven capillary flow for handling biological entities, such as chromatographic separation [26], protein-based diagnoses [27–30], and preparation of biological fluids [31].

Recently, reports have shown that the formation of the coffee ring is dependent on the shape of the suspended particles [32]. Compared with spherical particles that form perfect rings, anisotropic ellipsoids tend to stay at the air–water interface, where they experience strong particle–particle attraction and form a loosely packed structure that has higher resistance to the primary capillary flow. Consequently, rather than being concentrated at the periphery of the droplet, non-spherical ellipsoids become uniformly deposited after drying, showing their ability to suppress the coffee ring effect. Importantly, this shape-dependent suppression can be visualized without delicate environmental controls (humidity, temperature, or external pump). However, studies that exploit this phenomenon for biomedical detection have not been reported.

Here, we describe a method for the detection of nucleic acid using hybridization-induced suppression of the coffee ring effect. Our working principle is based on the phenomenon that non-spherical particles have higher resistance to the coffee ring formation, the schematics of which are shown in Fig. 1A. Suspended microspheres were surface-functionalized with single-strand DNA probes that can recognize a target DNA. Two types of probes, P1 (blue) and P2 (green), were designed to hybridize in juxtaposition with one target DNA (red). Using microspheres functionalized with either P1 or P2, the present target DNA hybridized simultaneously with both P1 and P2, leading to the generation of non-spherical particle agglomerates through inter-particle cross-linking. Thus, when the aspect ratio (α = length/width) of the suspended particles significantly increases (from $\alpha = 1$ for mono-dispersed microspheres to $\alpha > 1$ for particle agglomerates), the particle agglomerates can be deemed non-spherical to resist the capillary flow and to suppress the coffee ring formation.

In this proof-of-concept study, we establish a method of detection that is effectively sensitive at low concentrations of 10–100 nM, with a wide dynamic range from 10^{-5} M to 10^{-8} M, and sufficiently specific to distinguish sequences with a single mismatched nucleotide. In addition, the mechanistic insight underlying the suppression of the coffee ring effect was also elucidated by video microscopy and numerical simulations. In the present study, we show how the coffee ring effect was exploited to amplify the microscale binding events into changes of pattern formation at macroscale without cumbersome instrumentations, thus offering a simple, inexpensive, and user-friend interface for detection of nucleic acid.

Table 1
Sequences of single-strand DNA probes $P1_{rpoB}$ and $P2_{rpoB}$, the associated fully matched target rpoB, single mismatched target 3′, middle (Mid) and 5′, and fully mismatched target pagA, where the mismatch nucleotide is underlined.

Strand name	Sequence
rpoB	5′-ACTTGTGTCTCGTTTCTTCGATCCAAAGCG-3′
$P1_{rpoB}$	5′-AAACGAGACACAAGT-/biotin/-3′
$P2_{rpoB}$	5′-/biotin/CGCTTTGGATCGAAG-3′
3′	5′-ACTTGTGTCTCGTTACTTCGATCCAAAGCG-3′
Mid	5′-ACTTGTGACTCGTTTCTTCGATCCAAAGCG-3′
5′	5′-TCTTGTGTCTCGTTTCTTCGATCCAAAGCG-3′
pagA	5′-CTCGAACTGGAGTGAAGTGTTACCGCAAAT-3′

2. Materials and methods

2.1. Synthesis of target-recognizing microspheres

To detect the target DNA sequence (rpoB), the single-strand DNA probes, biotinylated oligonucleotide $P1_{rpoB}$ and $P2_{rpoB}$, were dissolved in Tris–ethylenediaminetetraacetic acid (Tris–EDTA) buffer. The sequence is listed in Table 1. For the suspended microspheres, we selected fluorescent polystyrene microspheres with a diameter of 1.04 μm (Excitation:Emission is 480:520 or 660:690; Bangslab, USA), which were coated with streptavidin so that the biotinylated probes $P1_{rpoB}$ and $P2_{rpoB}$ would attach to them through the strong streptavidin-biotin link. Seventy micrograms of microspheres were mixed with 5 μg of either $P1_{rpoB}$ or $P2_{rpoB}$ in the microsphere storage buffer. After incubation for 30 min at room temperature, the microspheres were washed three times with binding buffer containing 20 mM Tris, pH 7.5, 1 M NaCl, and 1 mM EDTA with 0.0005% Triton X-100.

2.2. Coffee ring detection

Ten microliter of the target DNA (rpoB) was prepared at a range of concentrations (10^{-5} M, 10^{-6} M, 10^{-7} M, 10^{-8} M, 10^{-9} M, and 0 M) in the hybridization buffer containing 10 mM Tris–HCl, 1 mM EDTA, and 1 M NaCl, pH 8.2, with 0.2% Tween-20. For the mismatch experiment, rpoB was replaced by oligonucleotide targets with a single mismatched sequence, labeled 3′, Mid, or 5′ according to the location of mismatch, or an oligonucleotide target, pagA, with a fully mismatched sequence (Table 1). The target solution was first mixed with 35 μg of microspheres functionalized with $P1_{rpoB}$. The duration of the hybridization between $P1_{rpoB}$ and the target DNA was 30 min. At the period of time, another 35 μg of microspheres functionalized with $P2_{rpoB}$ were added to 10 μL of pure hybridization buffer. Next, the microspheres functionalized with either $P1_{rpoB}$ or $P2_{rpoB}$ were mixed in 10 μL of hybridization buffer for 5 min, then repeatedly centrifuged ($13.8 \times g$ for 3 min) and re-suspended three times. The hybridization buffer was then replaced by deionized water, leaving 14 μL as the final volume to make a volume fraction of 0.5%. The microsphere solutions were then centrifuged and re-suspended in deionized water 6–10 times. For the coffee ring formation, the solution was dispensed on a microscopic slide and left for approximately 15 min until it dried under ambient conditions.

2.3. Image analysis

The coffee ring images and time-lapse videos were taken by Nikon TS-100 and Nikon Ti-E microscopy equipped with a color CCD and CoolSNAP Myo, respectively. An image processing program was developed in MATLAB for the automated analysis of coffee ring formation (Fig. A.1). The original images of ring patterns were first converted from RGB to grayscale. Using an image segmentation method, the largest segment was identified as the droplet region and the background was removed from the image. With the intensity histogram of the ring pattern, the dark peak intensity (red dot) and the bright peak intensity (blue dot) were detected (Fig. A.1B). We then found the valley (blue square) in between the two peaks. The threshold (red square) was defined as the intensity level to the left of the valley, where its frequency equals that of the valley plus 2% of that of the dark peak. Finally, the program applied the threshold to the image and computed the ratio of the number of dark pixels to the total number of pixels covering the droplet region as a quantitative measurement of the ring pattern.

2.4. Numerical simulation

We simulated the meniscus profile surrounding the microspheres at the air–water interface using the Surface Evolver software, which is based on the principle that the liquid surface deforms and evolves toward the minimal energy status by a gradient descent method. The total energy is shown as follows:

$$E_{\text{total}} = E_{\text{surface}} + E_{\text{G}}, \tag{1}$$

where E_{total} is the total energy of the model system, E_{surface} is the interfacial surface energy, and E_{G} is the gravitational energy of the model system. Using the Surface Evolver software, the initial settings of vertices, edges, and facets were defined (Fig. A.2A). The Surface Evolver meshed the model into small triangular elements (Fig. A.2B). During the evolving process, these elements were deformed and reshaped until the total energy E_{total} was minimized.

For an individual triangular facet element, the surface energy can be expressed as

$$E_{si} = \frac{T_i}{2}|\vec{s}_{i0} \times \vec{s}_{i1}|, \tag{2}$$

where E_{si} is the surface energy of the triangular facet element i, $\vec{s}_{i0}$ and $\vec{s}_{i1}$ are the two edge vectors of triangular facet element i, and T_i is the surface tension of facet element i, where the settings of T_i are classified into three types: (1) $T_i = T$ (constant, the surface tension of the air–water interface), (2) $T_i = T\cos\theta_c$ at the water–solid interface, where θ_c is the contact angle, and (3) $T_i = 0$ at the solid–air interface. As such, the total surface (E_{surface}) can be obtained as

$$E_{\text{surface}} = \sum_i E_{si} = \sum_i \frac{T_i}{2}|\vec{s}_{i0} \times \vec{s}_{i1}|, \tag{3}$$

In addition, the gravitational potential energy can be expressed as

$$E_{\text{G}} = \rho g \int\int_{\text{liquid surface}} \frac{1}{2} Z^2 \vec{k} \cdot \vec{d}A, \tag{4}$$

where ρ is liquid density, g is gravity, z is the coordinate of the z-axis, and $\vec{k}$ is the unit vector of the z-axis. The corresponding gravitational energy ($E_{\text{G}i}$) of each facet element i can be described as

$$E_{\text{G}i} = \frac{1}{4}\rho g Z^2 |\vec{k} \cdot (\vec{s}_{i0} \times \vec{s}_{i1})|, \tag{5}$$

Consequently, we can calculate E_{G} in the Surface Evolver as follows:

$$E_{\text{G}} = \sum_i E_{\text{G}i} = \sum_i \frac{1}{4}\rho g Z^2 \left|\vec{k} \cdot (\vec{s}_{i0} \times \vec{s}_{i1})\right|, \tag{6}$$

and the total energy (E_{total}) of the system can finally be expressed as

$$E_{\text{total}} = \sum_i \frac{T_i}{2}|\vec{s}_{i0} \times \vec{s}_{i1}| + \sum_i \frac{1}{4}\rho g Z^2 |\vec{k} \cdot (\vec{s}_{i0} \times \vec{s}_{i1})|, \tag{7}$$

Two models were implemented: one bi-sphere and one tri-sphere. For the bi-sphere model, two solid microspheres with

a diameter of 1 μm were used. For the tri-sphere model, we simulated a system consisting of a group of two agglomerated microspheres with a third microsphere. The third microsphere was placed along the conjugate axis with respect to the two-microsphere agglomerate. The contact angle of the microsphere was 30° and the liquid surface tension was set at 70 mN/m.

3. Results

3.1. Detection of nucleic acid

To evaluate our method, we selected the rpoB gene, a chromosomal marker with species-species sequences representing a pathogenic strain *Bacillus anthracis*. To recognize the target DNA rpoB, two single-strand DNA probes ($P1_{rpoB}$, blue, and $P2_{rpoB}$, green) were used, the sequences of which are complementary to half of the sequence of rpoB (red) (Fig. 1A). The sequence is summarized in Table 1. The probes were biotinylated at one end, so that they could bind to the microspheres coated with streptavidin. As such, rpoB would hybridize with $P1_{rpoB}$ and $P2_{rpoB}$ in juxtaposition and lead to non-spherical particle agglomeration. Thus, during the drying process, spherical microspheres ($\alpha = 1$) tend to flow outward to the periphery of the droplet and form a ring, whereas anisotropic particle agglomerates ($\alpha > 1$) are more uniformly deposited and suppress the coffee ring effect. Based on this concept, after drying in deionized water, a perfect coffee ring was formed when the target DNA was absent (Fig. 1B). In contrast, the presence of target DNA at a concentration of 10^{-5} M resulted in a strong suppression of the coffee ring effect (Fig. 1C). Rather than moving to the periphery of the droplet during the drying process, most of the microspheres were uniformly deposited at the end. This change in pattern formation was dramatic and can be observed by direct visual inspection, showing the validation of this working principle.

In addition to the qualitative visual readout, our method can also provide quantitative measurements of the concentration of the target DNA. As the target concentration decreases, the suppression of the coffee ring effect also decreases. At a target concentration of 10^{-6} M, the microspheres did not cover the entire area but remained to form a wide, dark band around the edge (Fig. 2A). As the concentration further decreased to 10^{-7} M, 10^{-8} M, and 10^{-9} M, the dark regions became smaller on average (Fig. 2B–D), showing the dependence of the coffee ring suppression on the target concentration.

An image processing technique was used to quantify the change in coffee ring formation at different target concentrations. The images were binarized with a threshold obtained by the histogram shape-based method (Fig. A.1). The ratio of the dark area to the total droplet area provided a quantitative measure of the coffee ring. As shown in Fig. 2E, the ratio at a concentration of 10^{-5} M was 0.77 ± 0.11, and decreased to 0.22 ± 0.03 when the target DNA was absent. When the target concentration was decreased from 10^{-5} M to 10^{-9} M, the average ratio showed a dependence of the proportion on the concentration. At a concentration of 10^{-9} M, the average ratio was 0.26 ± 0.073, which was slightly greater than that at 0 M. It shows that the detection has ultimate sensitivity at 10–100 nM.

3.2. Specificity

To examine the specificity of this method, three types of mismatched oligonucleotide targets were used with a single mismatched nucleotide at 3′ end, 5′ end, or at the middle of the oligonucleotide sequence (Table 1). These three mismatched targets were applied at a concentration of 10^{-5} M. The suppression of the coffee ring effect was significantly reduced with the presence of these single mismatched targets (Fig. 3A–C) compared with the fully matched target (Fig. 1C). We also tested another oligonucleotide target, pagA, with a fully mismatched sequence at a concentration of 10^{-5} M. The result was very similar to the ring formation in the absence of target DNA (Figs. 3D and 1B). After image processing, the results from the null condition (target DNA absent), target DNA with a single mismatched sequence at 3′, 5′, or the middle, or target DNA with a fully mismatched sequence (pagA) showed significant differences from the results of the perfectly matched target, rpoB ($p < 0.0001$ for all cases; Fig. 3E). These results demonstrate that the method has the high specificity to distinguish target DNA with a single mismatched or a fully mismatched sequence.

3.3. Video microscopy

To elucidate how the coffee ring effect was suppressed, we performed video microscopy. In the absence of the target DNA, the microspheres were efficiently carried by the outward capillary flow to the periphery of the droplet, either in bulk or along the air–water interface, resulting in a ring-shaped structure at the rim (Fig. 4A and B, and Video A.1 and 2). Only small numbers of microspheres were left in the inner area of the droplet. In contrast, when target DNA was present at a concentration of 10^{-5} M, many of the microspheres remained in the inner area without being carried to the periphery of the droplet (Fig. 4C and Video A.3). Notably, when the microspheres were traveling toward the periphery of the droplet, many of they were first trapped at the air–water interface (Fig. 4D and Video A.4). According to the observation of anisotropic ellipsoid in the coffee

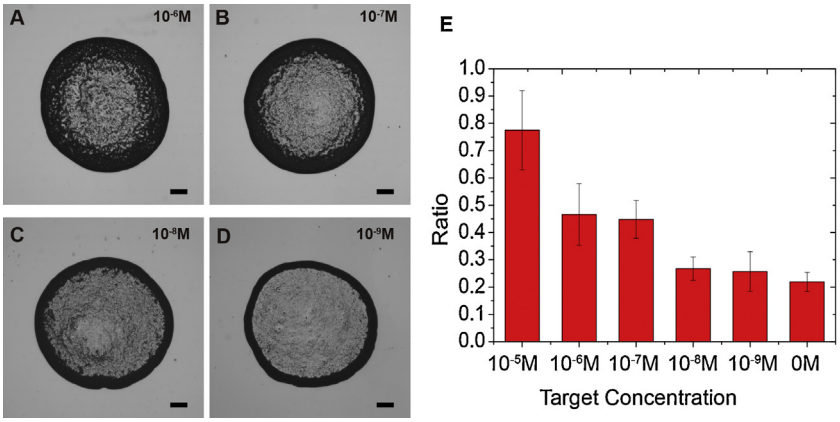

Fig. 2. Quantitative analysis of the ring formation reflecting the amount of target DNA. (A–D) The results for target DNA at concentrations of 10^{-6} M (A), 10^{-7} M (B), 10^{-8} M (C), and 10^{-9} M (D). Scale bar for (A–D), 250 μm. (E) The average ratio of the dark area to the total droplet area at different target concentrations ($n = 31$, 14, 24, 18, 18, and 33 rings for 10^{-5} M, 10^{-6} M, 10^{-7} M, 10^{-8} M, 10^{-9} M, and 0 M, respectively; mean ± SD; results from 2–4 independent experiments).

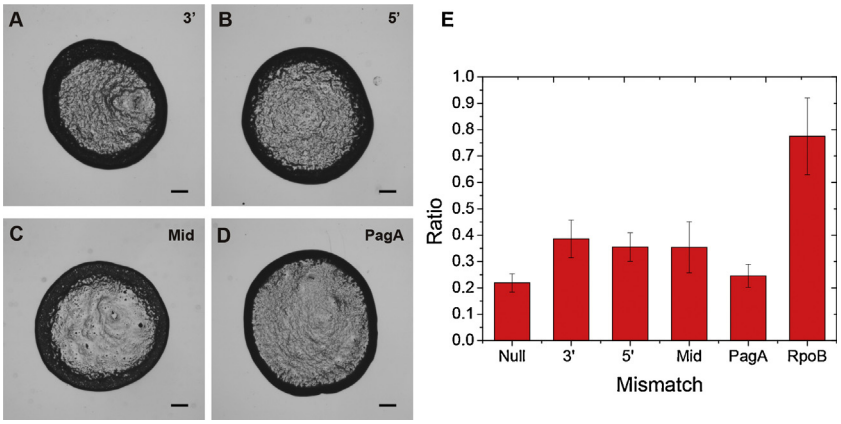

Fig. 3. Distinction of target DNA with a single mismatched sequence. (A–C) Coffee rings formed using target DNA with a single mismatched nucleotide at the 3′ end (A), the 5′ end (B), and a middle (C) location. (D) A coffee ring formed using a fully mismatched target, pagA. The target concentration is 10^{-5} M for all cases. Scale bar for (A–D), 250 μm. (E) The average ratio of the dark area to the total droplet area for rings using target DNA with a single mismatched sequence at 3′, 5′, or middle, or a fully mismatched sequence paA, compared with the null (target DNA absent) and fully matched sequence rpoB (n = 33, 18, 15, 16, 8, and 31 rings for null, 3′, 5′, Mid, pagA, and rpoB, respectively; mean ± SD; results from 2–4 independent experiments).

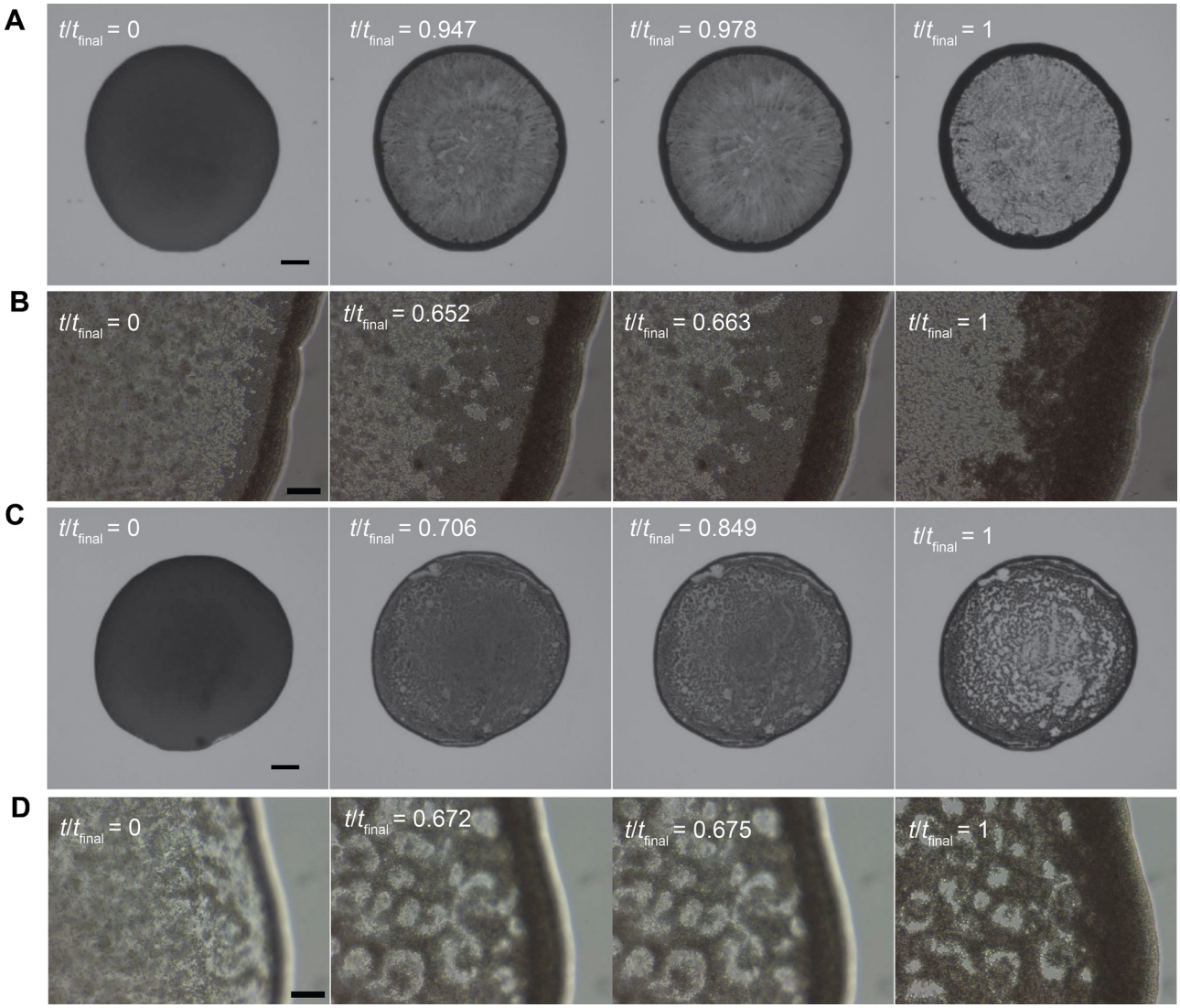

Fig. 4. Dynamics of the coffee ring formation. (A–B) In the absence of target DNA, the microspheres are carried toward the periphery of the droplet. (C–D) When target DNA is present at a concentration of 10^{-5} M, a significant number of microspheres remain inside the inner area, forming an interconnected network without being carried to the periphery of the droplet. Scale bar, 250 μm for (A and C) and 50 μm for (B and D).

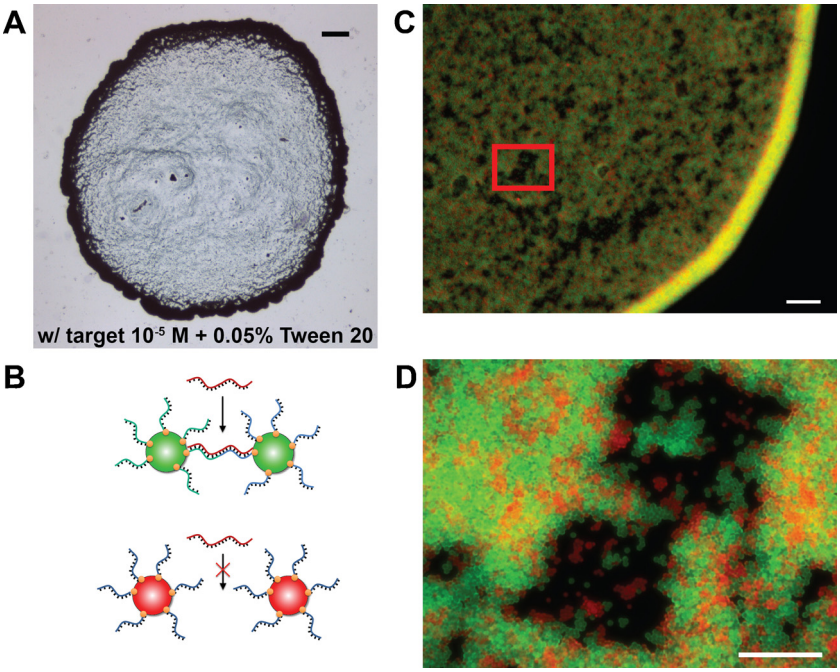

Fig. 5. Cheerios effect for coffee ring suppression. (A) In the presence of target DNA at 10^{-5} M, a perfect ring was formed when 0.05% Tween 20 was added into the final deionized solution. (B) Schematics of green fluorescent microspheres modified with $P1_{rpoB}$ or $P2_{rpoB}$ that can hybridize with rpoB; red fluorescent microspheres modified with non-relevant oligonucleotide probes. (C) The network structure formed jointly by green and red fluorescent microspheres. (D) Higher magnification images of the inset in (C). Scale bar, 250 μm for (A), 50 μm for (C), and 20 μm for (D). (For interpretation of the references to color in this figure legend, the reader is referred to the web version of this article.)

ring formation [32], this motion toward the air–water interface is caused by the outward capillary flow being blocked by the descending interface during evaporation. Later, the trapped microspheres adhered to each other, gradually forming a large network structure floating at the air–water interface (Fig. 4D and Video A.4). Although the microspheres underneath the air–water interface could still be carried toward the periphery of the droplet, the network structure at the air–water interface remained static, showing the enhanced fluidic resistance [32].

3.4. Cheerios effect

The coffee ring effect is suppressed by anisotropic ellipsoids because ellipsoids trapped at the air–water interfaces tend to deform the meniscus profile surrounding them [33]. This deformed meniscus profile later causes long-range and strong capillary attraction between particles [32,34,35], called the "Cheerios effect" [36]. The capillary attraction leads to the formation of a loosely packed structure that has increased surface viscosity over bulk viscosity and enhances fluidic resistance to the radially outward flows. Thus, this phenomenon prevents the suspended anisotropic particles from moving to the rim of the droplet and suppresses the coffee ring effect.

Our video microscopy revealed that the network structure was also formed at the air–water interface, which implies that, at the air–water interface, the anisotropic particle agglomerates in our system may also create the Cheerios effect, which produces long-range capillary attraction to other anisotropic particle agglomerates or other mono-dispersed microspheres. In other words, with some particle agglomeration initially generated by DNA hybridization, because of the deformed meniscus profile surrounding them, these particle agglomerates may later exert strong capillary attraction on other particles that do not bind with the target DNA, thereby causing additional attraction for particle connections.

To test this hypothesis, the deionized water in the final solution was supplemented with 0.05% Tween 20, a surfactant known to reduce the surface tension as well as the capillary attraction at the air–water interface. Consistently, although target DNA was present at a high concentration (10^{-5} M), a perfect ring was still formed when the surface tension was reduced (Fig. 5A), which supports our hypothesis that capillary attraction at the air-liquid interface plays an important role in the suppression of the coffee ring effect.

To further investigate whether the capillary attraction was applied to other mono-dispersed microspheres, we used fluorescent microspheres. Green fluorescent microspheres modified with single-strand DNA probes ($P1_{rpoB}$ or $P2_{rpoB}$) were mixed with red fluorescent microspheres modified with non-relevant oligonucleotide probes (Fig. 5B). In the presence of the target DNA, rpoB, although the red fluorescent microspheres only carried a non-relevant oligonucleotide probe that does not hybridize with rpoB, they were still incorporated into the particle agglomerates formed by the green fluorescent microspheres (Fig. 5C and D). These results indicate that the particle agglomerates in the coffee ring formation can recruit microspheres that do not bind with the target DNA and jointly form the network structure that amplifies the fluidic resistance.

3.5. Numerical simulation

The Cheerios effect requires deformed air–water interface to trap the colloid particle and enhance the inter-particle capillary attraction. To investigate whether the air–water interface was deformed in the regions surrounding particle agglomerates, we calculated the interfacial shape surrounding the particle agglomerates. We first constructed a bi-sphere model using two microspheres with a different center-to-center distance L (Fig. 6A) to investigate the deformation of the meniscus profile before and after particle agglomeration. When L equaled three times the diameter of the microsphere d, where they were deemed to be

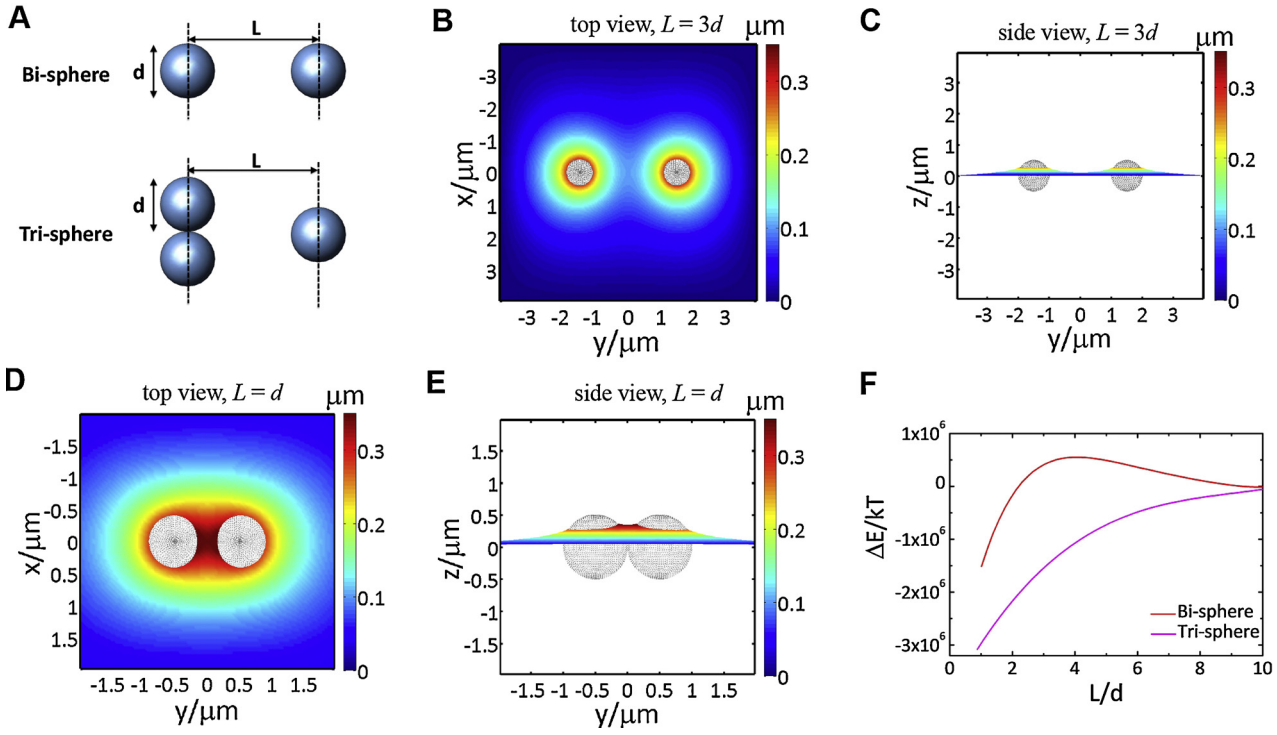

Fig. 6. Numerical simulation of the air–water interface surrounding the microspheres. (A) Schematics of the bi-sphere and tri-sphere models. (B) Top view of the air–water interface of the bi-sphere model for $L = 3d$. (C) Side view of the air–water interface of the bi-sphere model for $L = 3d$. (D) Top view of the air–water interface of the bi-sphere model for $L = d$. (E) Side view of the air–water interface of the bi-sphere model for $L = d$. The color map represents the interface height for (B–E). (F) For the bi-sphere and tri-sphere models, the potential energy ΔE plotted versus L/d with the reference position at $L/d = 10$. (For interpretation of the references to color in this figure legend, the reader is referred to the web version of this article.)

mono-dispersed microspheres, although the interface height in between the microsphere increased slightly, the triple contact lines on the microsphere remained flat (Fig. 6B and C). When L decreased to d, that is, the two spheres were in intimate contact with each other and were deemed to be a particle agglomerate, the contact lines were significantly distorted and no longer flat (Fig. 6D and E), and the interface height between the microspheres increased dramatically. This result shows that the particle agglomerate can induce a distinctive distortion of the meniscus profile.

To further validate whether the distorted meniscus was responsible for the increased long-range capillary attraction, we constructed a tri-sphere model. We hypothesized that the distorted meniscus surrounding the particle agglomerates may enhance the attraction force to a third, nearby microsphere. With two microspheres agglomerated, a third microsphere was placed along the conjugate axis of two microspheres. In this case, the separation distance L referred to the distance between the center of the third microsphere and contact points of the agglomerated microspheres (Fig. 6A). We calculated the potential energy ΔE (surface tension, gravity) with respect to the reference position $L = 10d$ for both the bi-sphere and tri-sphere models (Fig. 6F). For the bi-sphere model, ΔE reached a maximum when $L \sim 4d$, which shows that the interaction between two mono-dispersed microspheres is repulsive for $L > 4d$ and becomes attractive for $L < 4d$. If no prior mechanism such as DNA hybridization is used to force the initial particle agglomeration, an energy barrier occurs and prevents the microspheres from assembling and remaining mostly mono-dispersed. This therefore prevents the formation of the network structure at the air–water interface. In contrast, in the tri-sphere model, ΔE continued to decrease when $L \leq 10d$, which shows that, with an already existing particle agglomerate connected through DNA hybridization, this particle agglomerate attracts a third microsphere by long-range capillary attraction (longer than 10 times the particle diameter) through the deformed meniscus profile. The increased attraction favors the formation of a network structure and amplifies the fluidic resistance. Eventually, the coffee ring effect is suppressed.

4. Conclusion

In this paper, we demonstrated a powerful method for the detection of nucleic acid using the suppressed coffee ring effect. After particles agglomerate due to DNA hybridization, the distorted air–water interface traps the particle agglomerate and exhibits a long-range capillary interaction with another particle agglomerate or mono-dispersed microspheres. This enhanced particle–particle interaction results in the formation of a strong network structure at the air–water interface, eventually suppressing the coffee ring effect to reflect the presence of target DNA. Our method has effective sensitivity for target DNA at a low concentration of 10–100 nM with a wide dynamic range from 10^{-5} M to 10^{-8} M, and high specificity to distinguish a sequence with a single mismatched nucleotide.

To facilitate the hybridization process, we applied repeated centrifugation and re-suspension as the final step before dispensing the droplet. For the solution with target DNA, the suppression of the coffee ring effect was increased when more cycles were applied, and became stable without further change after 6–10 cycles (Fig. A. 3 and 4), which indicates that the particle agglomeration mediated by DNA hybridization can be facilitated via such cyclic motion to enhance the efficiency. In contrast, in the absence of target DNA (Fig. A.3 and 4), a perfect ring was still formed after the same number of cycles, which shows that the cyclic motion only speeds up the hybridization without introducing another type of non-specific agglomeration via another mechanism. Note that suppression of coffee ring effect can be still achieved by static incubation for 1 h without applying the centrifuge/re-suspension cycles (Fig. A.5).

Furthermore, in consideration of low-resource settings, the centrifuge process can be applied by the use of an egg beater [37], which is compatible with resource-limited scenario.

This approach has many advantages over existing technologies. First, the use of the coffee ring effect offers an extremely simple and economical method of detection. When self-driven capillary flow is used, the need for special fluidic controls, e.g., external pumps, valves, or microfluidic circuitry, is eliminated. In addition, as the presence of target DNA is translated into a change in macroscopic patterns, i.e., from concentrated rings to the uniform deposition of particles, the readout becomes a macroscopic pattern that can be visualized directly. This avoids the requirement of specific readers such as a current meter, spectrometer, or fluorescence microscope. Therefore, with its portability, cost-effectiveness, energy efficiency, and user-friendly interface, this method provides great potential for portable testing and examination in the simpler fashion for resource limited settings.

Acknowledgements

We are pleased to acknowledge the support from National Natural Science Foundation of China (Grant No. 51305375). M. L. Lam is supported by Croucher Foundation (Grant No. 9500016) and City University of Hong Kong (Grant No. 7004160).

Appendix A. Supplementary data

Supplementary data associated with this article can be found, in the online version, at http://dx.doi.org/10.1016/j.snb.2014.09.006.

References

[1] Y. Li, M.A.R. St John, X.F. Zhou, Y. Kim, U. Sinha, R.C.K. Jordan, et al., Salivary transcriptome diagnostics for oral cancer detection, Clin. Cancer Res. 10 (2004) 8442–8450.
[2] N.L. Rosi, C.A. Mirkin, Nanostructures in biodiagnostics, Chem. Rev. 105 (2005) 1547–1562.
[3] F. Wei, P.B. Lillehoj, C.M. Ho, DNA diagnostics: Nanotechnology-enhanced electrochemical detection of nucleic acids, Pediatr. Res. 67 (2010) 458–468.
[4] Y.P. Ho, M.C. Kung, S. Yang, T.H. Wang, Multiplexed hybridization detection with multicolor colocalization of quantum dot nanoprobes, Nano Lett. 5 (2005) 1693–1697.
[5] K.W. Hsieh, A.S. Patterson, B.S. Ferguson, K.W. Plaxco, H.T. Soh, Rapid sensitive, and quantitative detection of pathogenic dna at the point of care through microfluidic electrochemical quantitative loop-mediated isothermal amplification, Angew. Chem. Int. Ed. 51 (2012) 4896–4900.
[6] T. Sato, A. Takayanagi, K. Nagao, N. Tomatsu, T. Fukui, M. Kawaguchi, et al., Simple PCR-based dna microarray system to identify human pathogenic fungi in skin, J. Clin. Microbiol. 48 (2010) 2357–2364.
[7] D.E. Garcia, T.H. Chen, F. Wei, C.M. Ho, A parametric design study of an electrochemical sensor, J. Lab. Autom. 15 (2010) 179–188.
[8] A.K. White, M. VanInsberghe, O.I. Petriv, M. Hamidi, D. Sikorski, M.A. Marra, et al., High-throughput microfluidic single-cell RT-qPCR, Proc. Natl. Acad. Sci. U.S.A. 108 (2011) 13999–14004.
[9] P.B. Lillehoj, F. Wei, C.M. Ho, A self-pumping lab-on-a-chip for rapid detection of botulinum toxin, Lab. Chip. 10 (2010) 2265–2270.
[10] P.B. Lillehoj, M.-C. Huang, N. Truong, C.-M. Ho, Rapid electrochemical detection on a mobile phone, Lab. Chip. 13 (2013) 2950–2955.
[11] Z.Q. Yuan, J. Cheng, X.D. Cheng, Y. He, E.S. Yeung, Highly sensitive DNA hybridization detection with single nanoparticle flash-lamp darkfield microscopy, Analyst 137 (2012) 2930–2932.
[12] F. Xia, X.L. Zuo, R.Q. Yang, Y. Xiao, D. Kang, A. Vallee-Belisle, et al., Colorimetric detection of DNA, small molecules, proteins, and ions using unmodified gold nanoparticles and conjugated polyelectrolytes, Proc. Natl. Acad. Sci. U.S.A. 107 (2010) 10837–10841.
[13] R. Elghanian, J.J. Storhoff, R.C. Mucic, R.L. Letsinger, C.A. Mirkin, Selective colorimetric detection of polynucleotides based on the distance-dependent optical properties of gold nanoparticles, Science 277 (1997) 1078–1081.
[14] S.K. Rastogi, C.M. Gibson, J.R. Branen, D.E. Aston, A.L. Branen, P.J. Hrdlicka, DNA detection on lateral flow test strips: enhanced signal sensitivity using LNA-conjugated gold nanoparticles, Chem. Commun. 48 (2012) 7714–7716.
[15] Q. Dai, X. Liu, J. Coutts, L. Austin, Q. Huo, A one-step highly sensitive method for DNA detection using dynamic light scattering, J. Am. Chem. Soc. 130 (2008) 8138–8139.
[16] M.Y. Han, X.H. Gao, J.Z. Su, S. Nie, Quantum-dot-tagged microbeads for multiplexed optical coding of biomolecules, Nat. Biotechnol. 19 (2001) 631–635.
[17] R.D. Deegan, Pattern formation in drying drops, Phys. Rev. E 61 (2000) 475–485.
[18] R.D. Deegan, O. Bakajin, T.F. Dupont, G. Huber, S.R. Nagel, T.A. Witten, Capillary flow as the cause of ring stains from dried liquid drops, Nature 389 (1997) 827–829.
[19] H. Hu, R.G. Larson, Evaporation of a sessile droplet on a substrate, J. Phys. Chem. B 106 (2002) 1334–1344.
[20] X.Y. Shen, C.M. Ho, T.S. Wong, Minimal size of coffee ring structure, J. Phys. Chem. B 114 (2010) 5269–5274.
[21] J. Park, J. Moon, Control of colloidal particle deposit patterns within picoliter droplets ejected by ink-jet printing, Langmuir 22 (2006) 3506–3513.
[22] S. Choi, S. Stassi, A.P. Pisano, T.I. Zohdi, Coffee-ring effect-based three dimensional patterning of micro/nanoparticle assembly with a single droplet, Langmuir 26 (2010) 11690–11698.
[23] H. Hu, R.G. Larson, Marangoni effect reverses coffee-ring depositions, J. Phys. Chem. B 110 (2006) 7090–7094.
[24] B.M. Weon, J.H. Je, Capillary force repels coffee-ring effect, Phys. Rev. E 82 (2010) 015305(R).
[25] T. Kajiya, W. Kobayashi, T. Okuzono, M. Doi, Controlling the drying and film formation processes of polymer solution droplets with addition of small amount of surfactants, J. Phys. Chem. B 113 (2009) 15460–15466.
[26] T.S. Wong, T.H. Chen, X.Y. Shen, C.M. Ho, Nanochromatography driven by the coffee ring effect, Anal. Chem. 83 (2011) 1871–1873.
[27] J.R. Trantum, D.W. Wright, F.R. Haselton, Biomarker-mediated disruption of coffee-ring formation as a low resource diagnostic indicator, Langmuir 28 (2012) 2187–2193.
[28] J.T. Wen, C.-M. Ho, P.B. Lillehoj, Coffee ring aptasensor for rapid protein detection, Langmuir 29 (2013) 8440–8446.
[29] C.P. Gulka, J.D. Swartz, J.R. Trantum, K.M. Davis, C.M. Peak, A.J. Denton, et al., Coffee rings as low-resource diagnostics: detection of the malaria biomarker plasmodium falciparum histidine-rich protein-II using a surface-coupled ring of Ni(II)NTA gold-plated polystyrene particles, ACS Appl. Mater. Inter. 6 (2014) 6257–6263.
[30] J.R. Trantum, M.L. Baglia, Z.E. Eagleton, R.L. Mernaugh, F.R. Haselton, Biosensor design based on Marangoni flow in an evaporating drop, Lab Chip 14 (2014) 315–324.
[31] H.M. Gorr, J.M. Zueger, J.A. Barnard, Lysozyme pattern formation in evaporating drops, Langmuir 28 (2012) 4039–4042.
[32] P.J. Yunker, T. Still, M.A. Lohr, A.G. Yodh, Suppression of the coffee-ring effect by shape-dependent capillary interactions, Nature 476 (2011) 308–311.
[33] D. Stamou, C. Duschl, D. Johannsmann, Long-range attraction between colloidal spheres at the air–water interface: the consequence of an irregular meniscus, Phys. Rev. E 62 (2000) 5263–5272.
[34] J.C. Loudet, A.M. Alsayed, J. Zhang, A.G. Yodh, Capillary interactions between anisotropic colloidal particles, Phys. Rev. Lett. 94 (2005) 018301.
[35] J.C. Loudet, A.G. Yodh, B. Pouligny, Wetting and contact lines of micrometer-sized ellipsoids, Phys. Rev. Lett. 97 (2006) 018304.
[36] D. Vella, L. Mahadevan, The Cheerios effect, Am. J. Phys. 73 (2005) 817–825.
[37] A.P. Wong, M. Gupta, S.S. Shevkoplyas, G.M. Whitesides, Egg beater as centrifuge: isolating human blood plasma from whole blood in resource-poor settings, Lab. Chip. 8 (2008) 2032–2037.

Biographies

Yuanhang Li received his bachelor's degree in Electronic Engineering from City University of Hong Kong in 2014. Currently he is pursuing his Ph.D. degree at University of California, Irvine under supervision of professor William Chi-Keung Tang.

Zichen Zhao received his bachelor's degree in Nuclear Engineering, University of Science & Technology of China (USTC) in 2013. Currently he is a Ph.D. candidate at Department of Mechanical and Biomedical Engineering, City University of Hong Kong.

Miu Ling Lam is currently an assistant professor in the School of Creative Media, City University of Hong Kong. She received her Ph.D. in Automation and Computer-Aided Engineering from The Chinese University of Hong Kong. In 2008-2010, she was a Croucher postdoc fellow in the California NanoSystems Institute at University of California Los Angeles specialized in Bioinformatics. Her current research focuses on cloud robotics, bioinformatics, RGB-D perception, wearables and interactive media.

Wei Liu received her B.Sc. in Mechanical Engineering, Xi'an Jiaotong University, China in 2002 and M.Sc. in Mechanical Engineering, Xi'an Jiaotong University, China in 2005. Currently she is a Ph.D. candidate at Department of Mechanical and Biomedical Engineering, City University of Hong Kong.

Pak Piu Yeung is currently studying in his BS degree in Bioengineering at City University of Hong Kong. His research interest focuses on development of biosensors.

Ching-Chang Chieng has been a professor of Engineering and System Science Department, National Tsing Hua University, Hsinchu, Taiwan since 1981. She is currently a visiting professor of Department of Mechanical and Biomedical Engineering, City University of Hong Kong. Her major emphasis of research is microscale heat transfer and fluid flow in recent years. Her specialties include numerical scheme developments and applications for turbulent flow computations, in both macro- and micro-scales. She obtained her Ph.D. in aerospace and ocean engineering from

Virginia Polytechnic Institute and State University in 1974. She is also an associate Fellow of AIAA.

Ting-Hsuan Chen received the BS degree in power mechanical engineering and the MS degree from the Institute of Microelectromechanical Systems from National Tsing Hua University, Taiwan. He obtained his Ph.D. in Mechanical Engineering from University of California, Los Angeles in 2012. In his Ph.D. dissertation, he focused on cellular left-right symmetry breaking of vascular stem cells and engineer approaches for tissue architecture. Since 2012, he has been an assistant professor at Department of Mechanical and Biomedical Engineering, City University of Hong Kong. His research interest is leveraging the microtechnology for biomedical applications, such as wettability control, biosensors, and cell mechanics.